Cell and Tissue Research (2021) 383:735–750
https://doi.org/10.1007/s00441-020-03284-9

REGULAR ARTICLE

Role of bone 1stem cell–seeded 3D polylactic acid/polycaprolactone/hydroxyapatite scaffold on a critical-sized radial bone defect in rat

Sonia Sahvieh[1] · Ahmad Oryan[1] · Shadi Hassanajili[2] · Amir Kamali[1]

Received: 17 March 2020 / Accepted: 14 August 2020 / Published online: 14 September 2020

Abstract

Osteoconductive biomaterials were used to find the most reliable materials in bone healing. Our focus was on the bone healing capacity of the stem cell–loaded and unloaded PLA/PCL/HA scaffolds. The 3D scaffold of PLA/PCL/HA was characterized by scanning electron microscopy (SEM), rheology, X-ray diffraction (XRD), and Fourier transform-infrared (FT-IR) spectroscopy. Bone marrow stem cells (BMSCs) have multipotential differentiation into osteoblasts. Forty Wistar male rats were used to organize four experimental groups: control, autograft, scaffold, and BMSCs-loaded scaffold groups. qRT-PCR showed that the BMSCs-loaded scaffold had a higher expression level of CD31 and osteogenic markers compared with the control group ($P < 0.05$). Radiology and computed tomography (CT) scan evaluations showed significant improvement in the BMSCs-loaded scaffold compared with the control group ($P < 0.001$). Biomechanical estimation demonstrated significantly higher stress ($P < 0.01$), stiffness ($P < 0.001$), and ultimate load ($P < 0.01$) in the autograft and BMSCs-loaded scaffold groups compared with the untreated group and higher strain was seen in the control group than the other groups ($P < 0.01$). Histomorphometric and immunohistochemical (IHC) investigations showed significantly improved regeneration scores in the autograft and BMSCs-loaded scaffold groups compared with the control group ($P < 0.05$). Also, there was a significant difference between the scaffold and control groups in all tests ($P < 0.05$). The results depicted that our novel approach will allow to develop PLA/PCL/HA 3D scaffold in bone healing via BMSC loading.

Keywords Bone marrow stem cells · Bone regeneration · PLA/PCL/HA scaffold · Tissue engineering · Radial bone

Introduction

Trauma, tumor resection, and bone infections cause massive bone defects that are not easily regenerated. Finding a proper method to improve the regeneration process is challenging for researchers and orthopedic surgeons (Oryan et al. 2014; Alidadi et al. 2017; Yu et al. 2019). For these types of defects, bone tissue engineering, which is the combination of biomaterials and cells, could be a new approach to bone regeneration and promotes fracture healing (Yu et al. 2019). As an ideal bone substitute, designing a new three-dimensional (3D) scaffold that contains both growth factors and stem cells has been challenging in regenerating critical-sized bone defects without side effects (Peter et al. 2010; Busilacchi et al. 2013; Shimojo et al. 2015; Sivashankari and Prabaharan 2016). Ceramics, polymers, and metals are the most critical materials utilized in the fabrication of bioscaffolds. However, the metallic and ceramic scaffolds have several limitations, including weak bone regeneration due to inordinate rigid fixation or poor degradability with brittle structure (Papadimitropoulos et al. 2013; Pilia et al. 2013; Inzana et al. 2014; Wang et al. 2015; Solgi et al. 2015; Shahrezaee et al. 2018a). Some synthetic and natural biomaterials such as chitosan, alginate/hydroxyapatite, polylactidecoglycolide (PLGA), and gelatin have been used as bone graft substitutes because they are non-toxic, are low-antigenic, and have good biocompatibility and biodegradability properties (Oryan et al. 2014, 2017a, 2018; Yu et al. 2019).

Natural biomaterials like hydroxyapatite (HA), which is formed by 30% collagen type 1 and 70% HA, are perfect

✉ Ahmad Oryan
oryan@shirazu.ac.ir

[1] Department of Pathology, School of Veterinary Medicine, Shiraz University, Shiraz, Iran

[2] Department of Chemical Engineering, School of Chemical and Petroleum Engineering, Shiraz University, Shiraz, Iran

biomaterials for fabrication of the scaffolds because they resemble bone tissue structure. Moreover, HA could enhance mesenchymal stem cell proliferation, as well as their osteogenic differentiation (Witzler et al. 2019). This biomaterial has two synthetic and natural origins; both sections have shown biodegradability, biocompatibility, and crystallinity characteristics, and it appropriately adheres to the bone tissue to facilitate bone regeneration (Eftekhari et al. 2018; Kumar et al. 2018). On the other hand, HA has some limitations, such as low porosity and brittle conformation in manufacturing bone scaffolds. For proper angiogenesis, the designed scaffold should have macro-pores and micro-pores; therefore, it should be fabricated by salt leaching, hydrogel, electrospinning, 3D printing techniques, and so on. Based on 3D printing, the pore size and porosity of the ultimate scaffold would be controlled better, which finally causes the best environment for the cells to grow and migrate (Babczyk et al. 2014; Ottensmeyer et al. 2018; Götz et al. 2019).

Poly(ε-caprolactone) (PCL), poly(lactic acid) (PLA), poly(lactic glycolic acid) (PLGA), and their blends are commonly used as common synthetic biomaterials because of their biodegradable properties (Pizzicannella et al. 2019). Among the synthetic biomaterials, PLA possesses unique characteristics such as ideal biodegradability, biocompatibility, mechanical properties, thermal plasticity, porosity, and appropriate cell ingrowth characteristics (Lopes et al. 2012; Gregor et al. 2017). PCL is another synthetic polymer which has a great potential to be used in orthopedic surgery (Eftekhari et al. 2018). However, this material also has some limitations, such as hydrophobicity, induction of fibrous encapsulation (in vivo), and slow biodegradability; therefore, it could be a good idea to reduce these limitations by coating the surface and blending it with other materials (Siddiqui et al. 2018; Marins et al. 2019; Zhang et al. 2019a). PLA/PCL scaffold can be utilized in bone regeneration programs; however, due to the lack of osteoinductivity of PLA/PCL, it should be incorporated with other osteoinductive materials and bioactive molecules to achieve proper ability in regenerating bone defects (Shahrezaee et al. 2018b).

The bone marrow mesenchymal stem cells (BMSCs) are the non-hematopoietic stem cells of bone marrow with multipotential differentiation ability, which are generally used for cell therapy in tissue engineering and regenerative medicine (Fu et al. 2019). Some characteristics of BMSCs, including low immunogenicity and high in vitro amplification capacity, are well-known criteria, making this cell line a proper alternative for bone regeneration (Hashimoto et al. 2019; Luo et al. 2019). Additionally, BMSCs have a great potential to differentiate into osteoblasts, which are considered as an important element in bone healing with cell-loaded scaffolds (Hou et al. 2019).

In this study, the bone healing capacity of PLA/PCL/HA scaffold, which was built by a unique method, including a combination of freeze-drying and an indirect 3D printing approach, was examined in vitro and in vivo. We also evaluated the impact of BMSCs on bone regeneration of critical-sized radial defects through loading BMSCs into the PLA/PCL/HA scaffold. Finally, the results of different experimental groups were comparatively evaluated, using biomechanical analysis, radiology, gross pathology, immunohistochemistry, computed tomography (CT), histopathology, and histomorphometry.

Materials and methods

Designing and preparation of the scaffold

The molecular weight of poly(lactic acid) (PLA) (MG Chemical, USA) and polycaprolactone (PCL) pellets (Sigma-Aldrich) was 120,000 and 70,000 to 90,000 g/mol, respectively. 99.8% chloroform solvent, hydroxyapatite particles (with 100 nm diameter), and D-fructose were provided from the Merck Co., Germany. The mold, which contained a hollow cavity of $5 \times 5 \times 5$ mm^3 cubic-shape struts, was designed by Solidworks software so that the struts created channels in the cast scaffold with 900-μm thickness. An indirect 3D printer (ZMorph Co.), with the 0.3-mm nozzle size, was used to make the scaffold. All the materials were dried in the vacuum oven for about 24 h. Composite suspensions of PLA/PCL/HA were then prepared by incorporating the ingredients in chloroform with the 10% *w/v* concentration of polymers. PLA was firstly added into the chloroform solvent and stirred at 25 °C for 1 h until it was thoroughly dissolved. The process of fabrication continued by adding PCL and stirring for 1 h and then fructose was added and mixed for 1 h. The weight ratio of PLA/PCL was 50/50. The final solution was mixed with HA (35 wt%) for almost 3 h to provide asymmetric distribution of the HA particles in the solution. The resultant suspension was poured into the negative mold, steadily and slowly. The mold was placed at − 80 °C, for 24 h, to be frozen and then freeze dried for another 24 h to remove the solvent. To leach out the fructose particles from the ultimate sample and to prepare the porous scaffold structure, the sample was taken out of freeze dryer. The fabricated scaffold was then left in the double-distilled water for 48 h and finally located in a vacuum oven for 24 h to evaporate the residual water content.

Energy-dispersive X-ray spectroscopy and scanning electron microscopy

The pore size, microstructure of the internal and surface structure of the scaffold, and morphological characterization of the adhered cells were determined by SEM images from TESCAN-Vega 3 SEM system. The ImageJ software (Image Ja ll platforms) was used to achieve the pore sizes by measuring 100 pores in the scaffold. After fixing in 2.5%

glutaraldehyde, dehydration by a graded concentration of ethanol (20, 40, 60, 80%, and absolute), osmium tetroxide processing, and gold coating, the morphology of BMSCs seeded into the scaffolds was determined after 24 h post-seeding. Using energy-dispersive X-ray spectroscopy (EDS), presence of HA, as well as the elemental analysis of scaffold, was evaluated.

Evaluation of porosity

The liquid displacement method with ethanol was performed to determine porosity of the scaffold (Mou et al. 2011; Torres et al. 2013). The scaffold was kept immersed in a specified volume of ethanol (v_1) in a graded cylinder until it commenced to float. The saturated scaffold and the total ethanol content were recorded as v_2. The ethanol saturated scaffold was then removed from the cylinder and the residual ethanol volume was reported as v_3 (Moghadam et al. 2017; Shahrezaee et al. 2018b). The scaffold volume was calculated by Eq. 1 and the scaffold porosity (%) was obtained according to Eq. 2.

$$V = (v_2 - v_1) + (v_1 - v_3) = v_2 - v_3 \quad (1)$$

$$\text{Porosity}\ (\%) = (v_1 - v_3)/(v_2 - v_3) \times 100 \quad (2)$$

Compression test

The compression test was performed to obtain the mechanical properties of the fabricated scaffold. The scaffold was compressed to a total strain of 80%, using 1 mm/min of compression speed and this process was repeated three times to gain the mean values, using a Zwick/Roell apparatus.

X-ray diffraction

The crystal structure of the pure PCL, HA, PLA, and its composite, PLA/PCL/HA, was characterized using the X-ray diffraction method (Raucci et al. 2010). This experiment was conducted and the data were achieved in 2θ angle range of 10–80° with an interval of 0.05° and a scanning rate of 3°/min.

Fourier transform infrared spectrometry

The functional groups and possible molecular interactions of the scaffold were identified by FTIR analysis, which was done by a NEXUS670 Fourier transform infrared spectrometer (wavelength 400–4000 cm^{-1}) (Bassi et al. 2011).

Degradation and pH analysis

The degradation rate was investigated at 37 °C in 0.01 M phosphate-buffered saline (pH = 7.4) at 7, 14, 21, 28, and 35 days post-incubation.The volume of the sample/buffered solution was 5%. The rate of degradation of the scaffold in PBS was estimated by Eq. 3 at different time intervals.

$$\begin{gathered} W_1 = \text{early dry sample weigh} \\ W_2 = \text{dry sample's weight after solution removal} \\ \text{Mass loss} = (W_1 - W_2)/W_1 \end{gathered} \quad (3)$$

The pH values were calculated and charted after each phase and the average of degradation behavior and porosity tests was evaluated by repeating these tests three times.

Rheology

The viscosity of PLA, PCL, and PLA/PCL blends was measured by the 25-mm diameter parallel plate (PP25) with 1-mm height gap, using a strain-controlled rheometer from Physica MCR 302, Anton Paar, Austria. The frequency sweep test was between 0.5 to 100 rad/s and conducted at 220 °C with 1% fixed shear strain, which was in the linear viscoelastic area of the sample (Ostafinska et al. 2015).

Cell seeding onto the PLA/PCL/HA scaffolds

To seed the BMSCs onto the scaffold, the sterilized scaffolds (UV light and 70% ethanol) were first located in 24-well tissue culture plates. The suspension of rat BMSCs (50 μL equivalent to 1.0×10^6 cells per 5-mm scaffold blocks) was then added on the top surface of the scaffolds and was incubated for 2 h to permit the cells to attach to the scaffolds.

Cell viability

The neutral red test was used to estimate cell viability by changing the culture medium with 0.0005% neutral red in normal saline at days 3, 7, and 10. In this step, the scaffolds were washed by normal saline and then fixed by calcium formol. Acid alcohol (1-mL acetic acid in 100 mL 50% alcohol) was used to elute the neutral red. The collected eluted dye was finally evaluated using a microplate reader (Bio-Tek Instruments, ELx800nb) and the optic density (550 nm wavelength) was considered as an index of the number of viable cells.

Quantitative real time-PCR analysis

The potential of a fabricated scaffold (PLA/PCL/HA) in inducing osteogenesis (OPN and OCN) and angiogenesis (CD31) was estimated by qRT-PCR on day 21. The RNeasy Micro Kit (Qiagen-74,004) was used to obtain the total RNA from the cells. Thereafter, the cDNA was synthesized, using Revert Aid First Strand cDNA Synthesis Kit (Fermentas, Sankt Leon-Rot, Germany, k1632) based on the manufacturer's protocols. Duplicate qRT-PCR reaction was done via the SYBR® Green PCR Master Mix (Applied Biosystems Life Technologies, REF 4367659) by the real-time PCR system (Applied Biosystems Life Technologies, ABiStepOnePlus). Finally, it was analyzed with StepOne software (Applied Biosystems, version 2.1). Comparative CT method (also known as the $2-\Delta\Delta Ct$ method) was used to relatively quantify gene expression, where some target genes were normalized to an endogenous control (GAPDH) and relative to calibrator group (2d cell culture flask). All samples were collected from three biological replicates.

Animals and surgical procedures

Forty adult male Wistar rats (225 ± 25 g) were generally anesthetized by 20 mg/kg ketamine hydrochloride plus 2 mg/kg xylazine (both from Alfasan, Holland). Via a 3-cm incision, the radial bone in both left and right forelimbs was then exposed and a 5-mm of diaphysis was osteotomized in each right and left radial bone by an electrical bone saw (Strong, Seoul, South Korea). The rats were randomly divided into 4 experimental groups: the defect group without any treatment (negative control group), the autograft group (positive control), the scaffold-treated group, and the group in which the defect was filled by the BMSCs-loaded scaffold ($n = 10$ rats in each group). The size of defect in all groups was $2 \times 2 \times 5$ mm^3, and the untreated group was considered as natural healing. Finally, subcutaneous injection of 5 mg/kg enrofloxacin (Irfan, Iran) and 1 mg/kg meloxicam (Razak, Iran) were used for 3 days as antibiotic therapy and post-operation analgesia, respectively.

Radiology, gross morphology, and computed tomography measurements

The animals were generally anesthetized on the lateral surface of radius at 40 and 80 days post-operation to estimate the percentage of gap closure. At the end of the study, all rats were euthanized and their radial bones were harvested. Then, CT scan investigation was done to calculate the rate of gap closure in different treatment groups. The 3D computed tomography scan images were prepared based on this supposition: *X* direction showed cranial/caudal, *Y* direction showed dorsoventral, and *Z* direction showed lateral/medial of the radius bone (the defect region was on the radius bone that was above the ulna bone). The regeneration capacity was scored by blindly gross macroscopic evaluation in all groups. The 0 scores were determined for the complete non-union bone defects and + 1, + 2, and + 3 were respectively considered for the presence of cracks within the defect (unstable union), incomplete union followed by cartilage or fibrous connective tissue, and the complete union followed by bridging bone (Oryan et al. 2012).

Histologic and histomorphometric studies

After decalcification of the bone samples by 10% EDTA (pH 7.4) for 35 days, all samples were embedded in paraffin wax and used for sectioning. The 5-μm tissue sections from the paraffin-embedded samples were then stained by hematoxylin and eosin (H&E). Finally, histomorphometric analyses were blindly scored by two independent pathologists to determine the number of fibrocytes, fibroblasts, chondrocytes, chondroblasts, osteocytes, osteoblasts, inflammatory cells, giant cells, and some constituents including the density of fibrous connective tissue, the newly formed cartilage, bone ingrowth, and the number of blood vessels, using Image-Pro Plus®V.6 (Media Cybernetics, Silver Spring, USA) (magnification × 400).

Immunohistochemical analysis

The unstained tissue sections were used to analyze the expression of primary antibodies such as osteocalcin (OC, ab13420, Abcam, MA) and CD31 (ab119339, Abcam, MA). The tissue sections were incubated in citrate buffer solution (Dako, Glostrup, Denmark) to heat-induce epitope retrieval at 60 °C overnight and were then blocked by 1% hydrogen peroxide for 30 min at room temperature. The slides were then incubated at 4 °C overnight with primary antibodies and the color reaction was developed, using 3,3′ diaminobenzidine and counterstained by hematoxylin. The tissue sections were studied using an ordinary light microscope (Olympus BX51; Olympus, Tokyo, Japan).

Biomechanical testing

The samples were wrapped in moist gauzes and kept at − 20 °C on the 80th day post-injury. Based on using 3-point bending test, the samples were settled on two supporting bars (16-mm distance) and the third bar was settled under midline of the defect area (Oryan and Alidadi 2018). Ultimately, the

samples were loaded (universal testing machine, Instron, London, UK) at the 5 mm/min rate until they were fractured. The load-deformation curve was drawn for strain, maximum stress, stiffness, and maximum load.

Statistical analysis

All quantitative data were analyzed by one-way analysis of variance (ANOVA) and Tukey post hoc tests subsequently. For analyzing qualitative data, Kruskal-Wallis and non-parametric ANOVA were used. If the scored values showed significant differences ($P < 0.05$), the Mann-Whitney U test was used for further analysis. All statistical analyses were recognized by GraphPad Prism software Version 8.2.0.

Results

Characterization of the scaffold

Based on the SEM ultramicrographs, the architecture of the macro-pores and micro-pores in the scaffold was shown with proper interconnectivity (Fig. 1a). After analyzing the ultramicrographs, the mean diameter of micropores in the scaffold was calculated 141.0 ± 47.0 μm and the average thickness of the pore walls was 27.87 ± 2.21 μm. The elemental analysis of the PLA/PCL/HA scaffold is shown in Fig. 2a. The results depicted the presence of Ca, P, C, and O at different points on the surface of the sample. Elemental analysis revealed that the weight ratio of Ca/P was near 1.8. The average of the scaffold porosity (%) was estimated about 69–71%. The stress-strain curve (Fig. 2b, (compressive modulus (MPa): 0.6339 ± 0.03995)) estimated the compressive behavior, which showed the linear behavior from the beginning of the diagram until 20% of strain and the slope of the diagram at 20–45% strain revealed collapse of the pores. After 45% strain, all pores thoroughly collapsed and the scaffold was densified. The crystallinity of different samples was studied using XRD test, the results of which are provided in Fig. 2c. The X-ray diffraction peaks in the HA sample were exhibited at 26°, 31.8°, 32.9°, 40°, and 49° with a hexagonal shape and lattice parameters of $a = 0.943$ nm, $b = 0.493$ nm, and $c = 0.688$ nm. The major diffraction peaks were seen at 2 = 16.6° and 2 = 18.9° for PLA and PCL; the reflections were at 2 = 21.6° and 2 = 23.8° with a lattice morphology similar to polyethylene (orthorhombic). The lattice parameters were $a = 0.948$ nm, $b = 0.498$ nm, and $c = 1.727$ nm. The above peaks were also observed in XRD pattern of PLA/PCL/HA with some changes. FTIR spectroscopy was done for PCL, HA, PLA/PCL/HA, and PLA samples (Fig. 2d). The FTIR results were considered based on the peak positions shown in Table 1. By comparing the given bands in pure materials with those in the PLA/PCL/HA spectrum, some shifts in the position of the peaks were noticeable (e.g., carbonyl and hydroxyl groups). The changes in pH (Table 2) showed that the HA nanoparticles result in buffering behavior. We observed that releasing alkaline ions of HA results in increased pH value, but releasing the acidic by-products of polymers into the solution results in decreased pH measurement.

The degradation behavior of the scaffold was related to some factors like material properties, microstructure, and porosity. The scaffold was degraded 2–2.5% in the neutral pH (in vitro) after 35 days (Table 3). This percentage of degradability provided a proper opportunity to allow the osteoblasts and osteocytes to migrate to the defect site before the scaffold was degraded thoroughly. In this scaffold, the highest, as well as the lowest degradation rate, belonged to PLA and PCL, respectively. The rheology test was done on PLA, PCL, and PLA/PCL (50/50) to analyze the viscoelastic behavior of the samples and was also used in drawing the diagram of the complex viscosity curve versus angular frequency (Fig. 2e). Figure 2f shows the results of a neutral red test, which states that the scaffold could initiate metabolism of the cells.

Morphology and adherence of BMSCs onto the scaffold

The isolated cells had phenotypes that were differentiated to adipogenic and osteogenic lineages and they were analyzed by the markers of their surface via flow-cytometry. The expression of the majority of BMSCs was positive for CD90 (> 90%) and CD25 (75%). Additionally, 20% of the cells expressed CD34, whereas only 5% expressed CD11b.

As can be seen in Fig. 1b, SEM ultramicrograph showed a successful adherence of BMSCs to the surface of scaffold. By the cell's pseudopodia, they were attached strongly to the porous scaffold surface 24 h following seeding.

qRT-PCR analysis

The expression level of osteogenic- and angiogenic-related genes of the BMSCs seeded on the PLA/PCL/HA scaffolds was analyzed by qRT-PCR after 21 days post-cell seeding (Fig. 3a–c). The BMSCs-loaded PLA/PCL/HA scaffold showed a significantly higher expression level of CD31 in comparison with the untreated (2D cell culture) group ($P < 0.05$). Moreover, the OPN expression level increased in the PLA/PCL/HA group in comparison with the control one ($P < 0.01$). OCN was also expressed higher in the PLA/PCL/HA group when compared with the control group ($P < 0.001$).

Evaluation of bone formation by gross morphology, radiology, and CT scan

As shown in Fig. 4a–a"', the gross views were analyzed on days 40 and 80 post-surgery (Fig. 4d–d"'). The control group

Table 1 FTIR spectra bands of PLA, PCL, and HA

	CH_2 symmetric stretch	Asymmetric stretch	Carbonyl stretch	C–O stretch	CH_3 stretch	PO_4^{-3} stretch	OH stretch
PCL	2940 cm^{-1}	2860 cm^{-1}	1720 cm^{-1}	Around 1160 cm^{-1}			
PLA			1740 cm^{-1}	1032 cm^{-1}	2883 cm^{-1}		
HA						Around 1036 cm^{-1}	3500 cm^{-1}

displayed unstable union, the scaffold group showed incomplete union, and the BMSCs-seeded scaffold group demonstrated complete union after 80 days post-operation (Table 4). Higher macroscopic scores belonged to the autograft and cell-seeded scaffold groups when compared with the control group ($P < 0.01$). The significant difference was also seen between the scaffold and non-treated groups ($P < 0.05$). On the other hand, there were no significant differences in the macroscopic union scores between the BMSCs-scaffold and autograft group ($P > 0.05$).

The radiographic images showed the healing process by the percentage closure of bone defect after 40 and 80 days post-injury. BMSCs enhanced fracture healing and there was a significant difference between the control and BMSCs-loaded scaffold groups ($P < 0.001$) (Fig. 4g–g').

Histopathologic, histomorphometric, and immunohistochemical analysis

The loose areolar connective tissue, together with the newly formed blood vessels, fibroblasts, and unorganized immature collagen fibers, existed in the defect site of the untreated group on the 40th day post-injury and a fibrovascular tissue filled the defect region in the untreated group at this stage (Fig. 5a–h). There was also a ridge of fibrocartilage tissue at the edges of the old bone on 80 days post-injury in the gap region of the animals of this group (Fig. 6a–h). Osseointegration just began on one side of the bone gap in four samples in the autograft group on the 40th day post-injury, but complete bone integration was visible at 80 days post-operation. The defect site was filled with fibrous connective tissue, which surrounded the scaffold residues in the scaffold and BMSCs-loaded scaffold groups on 40 days post-surgery. The scaffolds were degraded entirely after 80 days and the gap in the scaffold and BMSCs-loaded scaffold groups was covered with cartilage, fibrocartilage, fibrous connective tissue, and woven bone. The woven bone and fibrocartilage tissue filled the gap in the BMSCs-loaded scaffold group more than the other tissues and the remodeled compact bone was seen in this group after 80 days. Still, it was not observed in the scaffold group after this period.

The results of the histomorphometric evaluation depend on the density of fibrous (F), osseous (O), and cartilaginous (C) tissues. The highest density of osseous and cartilage tissues was seen in the BMSCs-seeded scaffold and autograft groups, which had a significant difference with the control group after 80 days post-injury ($P < 0.05$) (Table 5). The density of fibrous connective tissue was significantly higher in the non-treated group than the other groups ($P < 0.05$), and the density of bone ingrowth was significantly higher in the BMSCs-seeded and autograft groups in comparison with the empty defect either on 40 or 80 days post-injury ($P < 0.05$).

The osteogenic and angiogenic immunohistochemical (IHC) analyses in all groups are demonstrated in Fig. 7a–h. The OC expression level was significantly lower in the untreated group in comparison with other experimental groups ($P < 0.05$) and the endothelial marker, CD31, was significantly upregulated in the cell-free and BMSCs-seeded scaffolds compared with the control group ($P < 0.01$). The minimum level of OC and CD31 expressions was related to the control group ($P < 0.001$).

The results of biomechanical performance, including maximum strain (%), ultimate load (N), stiffness (N/mm), and stress (N/mm^2), are shown in Fig. 8a–d. All treated groups depicted higher maximum stress, ultimate load, and stiffness compared with the control group ($P < 0.01$) and the highest strain (%) was estimated for the untreated group in comparison with other groups ($P < 0.001$).

Table 2 The pH change at 7, 14, 21, 28, and 35 days

	Mean ± SD
7 days	7.606667 ± 0.025166
14 days	7.633333 ± 0.031316
21 days	7.576667 ± 0.025166
28 days	7.573333 ± 0.023094
35 days	7.543333 ± 0.030415

Discussion

Bone grafts have been used for bone regeneration, particularly in large bone defects due to pathologic occasions, fractures, and tumors. Still, the autologous bone remains as the gold standard therapy because of its superior capability to regenerate bone tissue and lack of the necessity for further surgery (Oryan et al. 2017b). Tissue engineering is the most reliable

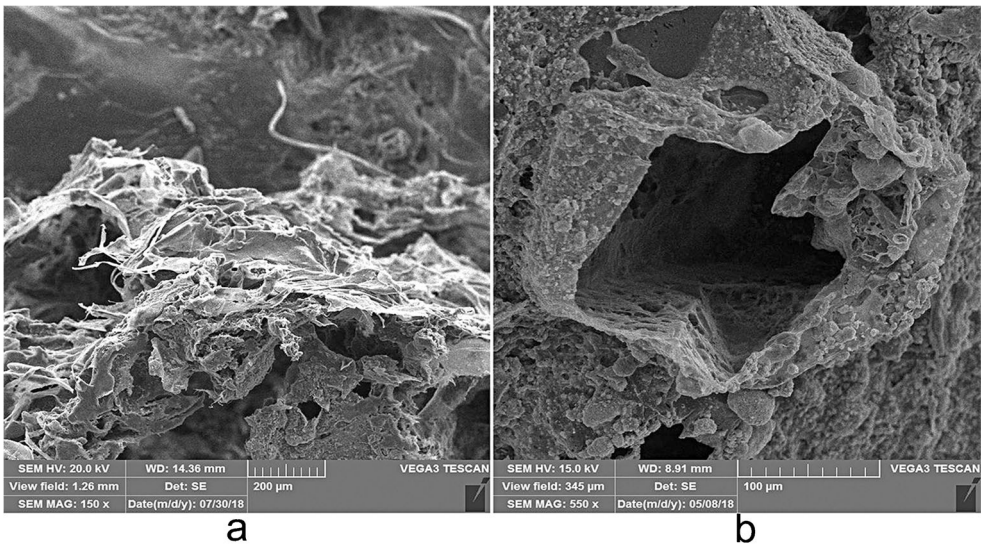

Fig. 1 **a** SEM ultramicrograph of the PLA/PCL/HA scaffold. It shows macro-pore, micro-pore, and ultrastructure of scaffold. **b** BMSCs loaded on the outer surface of the scaffold after 1-day seeding

method in bone engineering and regenerative medicine in the fields of reconstructive, plastic, and orthopedic surgeries. A combination of scaffolds and osteogenic and/or osteoinductive agents has been shown to result in enhanced and more efficient bone healing, particularly in large bone defects (Moshiri et al. 2013; Shahrezaie et al. 2017).

The PLA/PCL/HA scaffold could provide a suitable environment for cells to survive, adhere, proliferate, migrate, and differentiate to bone-forming cells, and the HA portion of the scaffold results in enhanced bone formation and earlier mineralization (Mondal et al. 2016; Gregor et al. 2017; Fang et al. 2019; Lima Cavalcanti et al. 2019). As the stoichiometric

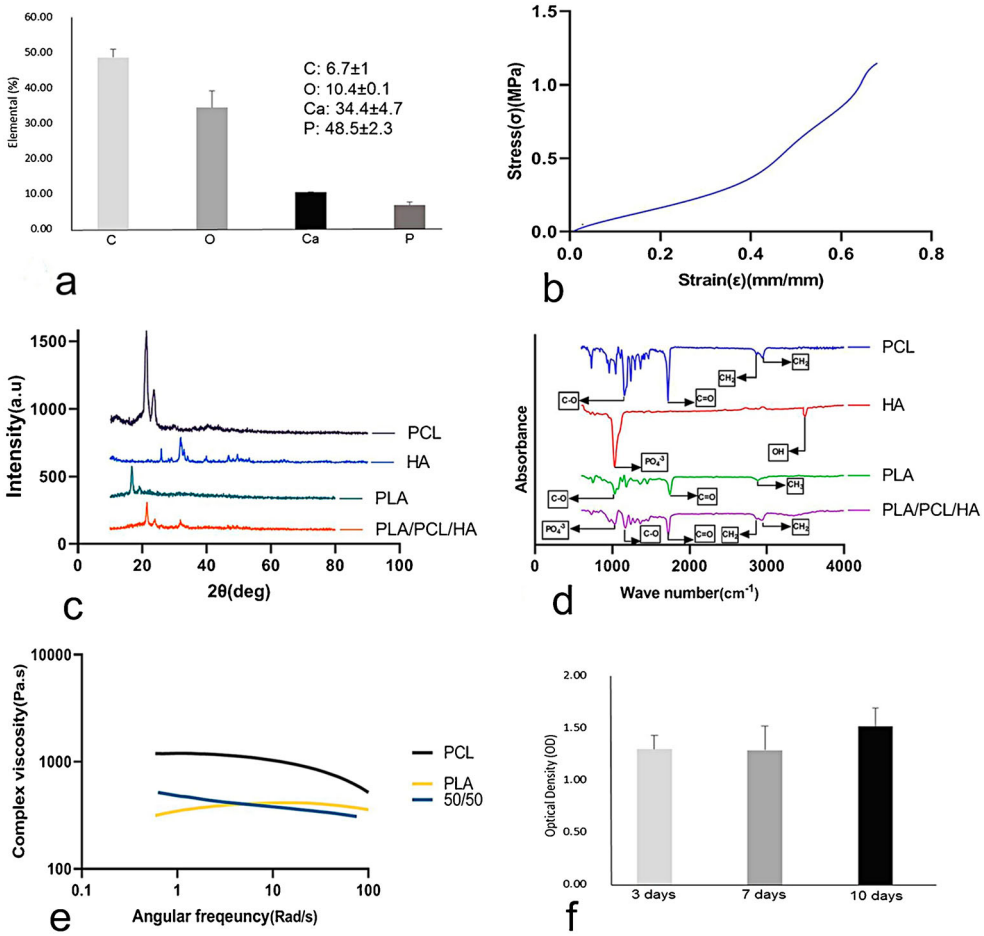

Fig. 2 **a** Elemental analysis of the scaffold. **b** Stress-strain diagram. **c** XRD patterns of the PLA/PCL/HA, PCL, PLA composites, and HA nanopowder. **d** FTIR diagram of PLA/PCL/HA, PCL, HA composites, and PLA nanopowder. **e** The complex viscosity variation in terms of angular frequency. **f** The results of neutral red for the PLA/PCL/HA scaffold

Table 3 The degradation rate of scaffold at 7, 14, 21, 28, and 35 days

	Mean ± SD
7 days	101.2291 ± 0.116372
14 days	100.7574 ± 0.002957
21 days	99.48005 ± 0.001224
28 days	98.72202 ± 0.003591
35 days	97.83563 ± 0.491151

value of Ca/P was about 1.8 in the hydroxyapatite molecule (Eshraghi and Das 2012), the results of our elemental analysis indicated the loading and attachment of HA at different parts of the scaffold. However, HA has low porosity, which makes its mechanical properties (e.g., fracture toughness) lower than normal bone and this limits its application, particularly in critical bone defects (Ramtani 2004; Ottensmeyer et al. 2018). Accordingly, we designed the scaffold with synthetic biomaterials that are more efficient in bone tissue engineering because of their higher mechanical strength and their solid structure in contrast to the biological implants (Vergroesen et al. 2011).

The results showed a suitable porosity of the fabricated scaffold (69–71%) which is necessary for cell infiltration, proliferation, and bone tissue ingrowth. Moreover, the pore size of the scaffold should be proportionate with the size of the tissue with which the scaffold is fabricated. The bone cell (osteoblast) size is around 20–50 μm, so based on this size, the preferred pore size should be 100–350 μm (Leonga et al. 2008). Our results were also confirmed with this manifesto.

The compressive behavior of the scaffold demonstrated all three stages based on Hassanajili and colleagues' study (Hassanajili et al. 2019): (1) Linear behavior of the diagram (elastic response), (2) the almost steady stress was due to the collapse of the pores in response to pressure, and (3) the scaffold densification. The XRD results indicated that PCL has higher crystallinity than pure PLA. PLA/PCL/HA 50/50–65/35 displayed nearly all characteristic peaks induced from HA loading in addition to the peaks of neat PLA and PCL. However, the PLA phase of composite displayed peaks with weak intensity and broadness, revealing that the crystallinity in the PLA phase was reduced. This phenomenon may be attributable to some interactions between PLA and HA. The result of FTIR showed the shifts of peak position might be attributed to hydrogen bonding interactions between the chemical groups of PLA and HA in the scaffold.

Table 4 Kruskal-Wallis non-parametric ANOVA. Complete non-union bone defect: (0), unstable union: (+ 1), incomplete union: (+ 2), and complete union: (+ 3). Day 40: $P < 0.05$ (1 vs. 3), $P < 0.01$ (1 vs. 2, 4). Day 80: $P < 0.05$ (1 vs.3), $P < 0.01$ (1 vs. 2, 4)

Group	Macroscopic score (day 40) Median (min-max)	Macroscopic score (day 80) Median (min-max)
Untreated defect (1)	0 (0–0)	1 (0–1)
Autograft (2)	2 (1–2)	3 (2–3)
Scaffold (3)	1 (1–2)	2 (1–2)
Scaffold + BMSCs (4)	2 (1–2)	3 (2–3)

Our results in pH changes agreed with the previous studies indicating that buffering behavior was because of the HA nanoparticles. So the impression swelling response of the degradation of acidic polymer would hinder these nanoparticles by an increase in pH value (Misra et al. 2009; Roohani-Esfahani et al. 2011). HA is also able to chemically bond to living bone and refines scaffold stiffness so it is a notably proper osteoinductive and osteoconductive material in bone healing (Schumacher et al. 2010; Yun et al. 2010). On the other hand, the application of more HA ingredients in such scaffolds results in reduced degradation rate (Hassanajili et al. 2019). Still, PLA has been shown to act as an appropriate degradable bone scaffold in previous studies and it degrades in lactic acid, which normally exists in body organs (Guntillake and Adhikari 2003; Gregor et al. 2017). Whereas because of the brittleness of PLA and HA, the application of PCL enhances the elasticity of scaffold. The rheology results showed the shear-thinning behavior in neat polymers and also their blend with the following zero shear viscosity trend: PCL > PLA/PCL (50/50) > PLA. This showed that the elasticity of PLA/PCL blend raised in the presence of PCL and proper elasticity should exist in the scaffold to apply it in bone tissue engineering.

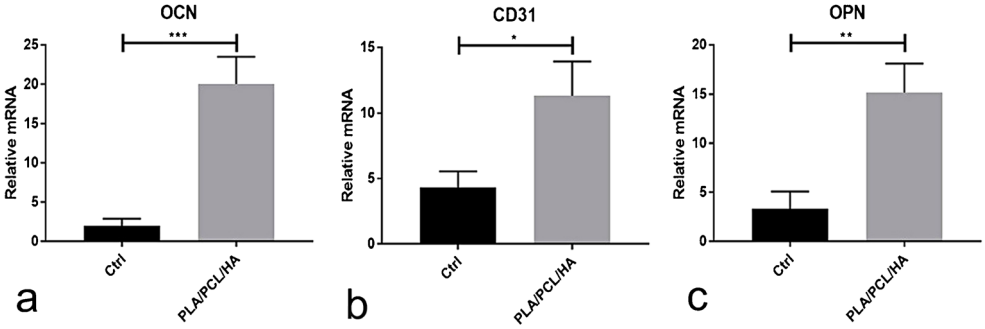

Fig. 3 The expression level of the CD31, OCN, and OPN genes analyzed by qRT-PCR at day 21 (**a**–**c**). The PLA/PCL/HA scaffold enhanced the expression level of all genes compared with the control group. *, **, ***: values indicate the significant differentiation in comparison with the control group, *$P < 0.05$, **$P < 0.01$, ***$P < 0.001$

Many studies have shown the therapeutic impressions and low cost of PCL scaffold in bone tissue engineering (Woodruff and Hutmacher 2010; Mitsak et al. 2011; Jensen et al. 2013; Cui et al. 2014; Kamath et al. 2014). Eftekhari and colleagues stated that PCL nanocomposite showed the highest value of union index, cortex index, bone marrow index, and spongiosa index between the untreated, HA-, and β-tricalcium phosphate–treated groups at 15, 30, and 45 days post-treating. The histopathological findings of the same study also showed that the quantity of newly lamellar bone formation was higher in the PCL nanocomposite–treated group than the other groups (Eftekhari et al. 2018). All these data suggest that PCL has beneficial effects on the bone healing processes, which could have great potential in tissue engineering and clinical applications.

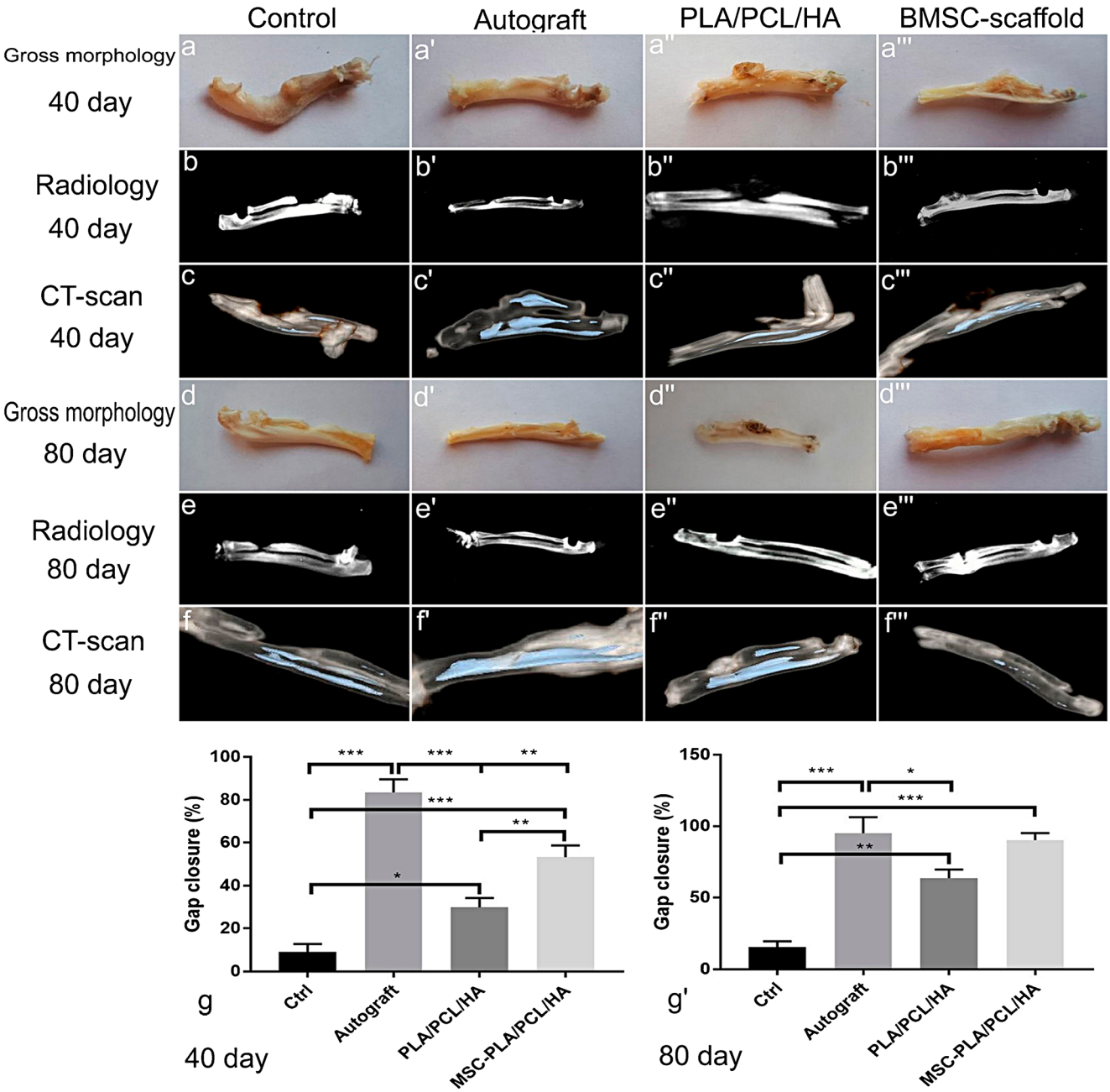

Fig. 4 Gross pathology of the healed defects of the rat radius bones on the 40th (a–a''') and 80th (d–d''') days post-surgery. The gap in the autograft, PLA/PCL/HA, and BMSCs-PLA/PCL/HA groups was almost replaced by hard tissues. The scaffold residues were seen in the defect sites in both PLA/PCL/HA and BMSCs-PLA/PCL/HA groups on the 40th day post-surgery. The radiographic images of the healing defect on the 40th (b–b''') and 80th (e–e''') days post-injury. The CT-scan images of the defect area on the 40th (c–c''' and 80th (f–f''') days post-operation and the radiographic measurements of the gap closure (%) in different experimental groups (g–g'). *, **, ***: values indicate the significant differentiation in comparison with the control group, $*P < 0.05$, $**P < 0.01$, $***P < 0.001$

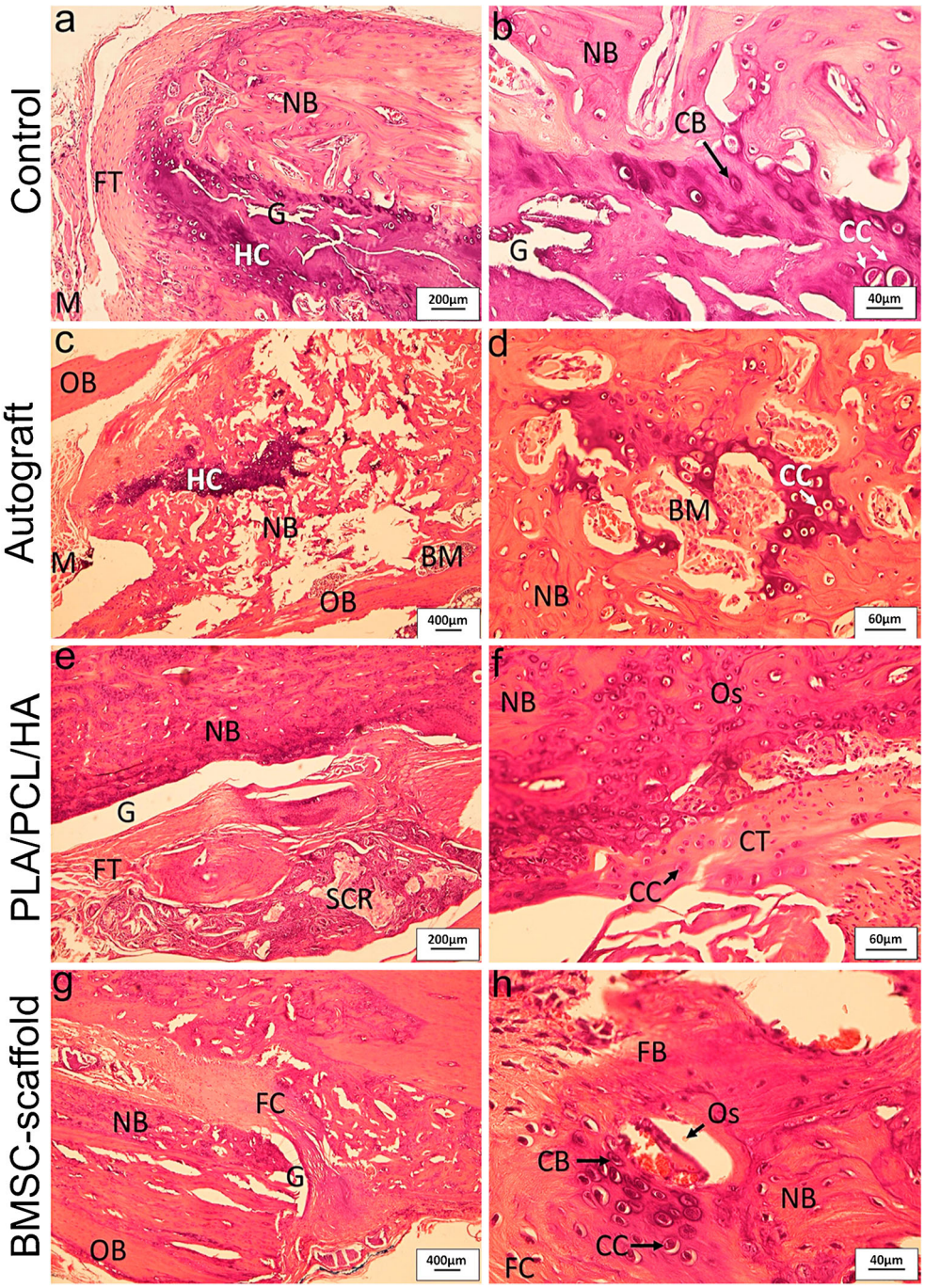

Fig. 5 Histopathological sections of the radius bone defects of rats after 40 days post-surgery (a–h). The defects in the PLA/PCL/HA group were mostly filled by the cartilage tissue. The defects in the BMSCs-PLA/PCL/HA group were replaced with new tissues containing fibrous, cartilage, and bone tissues and the scaffold was thoroughly degraded. The least amount of healing in the defect region was seen in the control group. NB new bone, BM bone marrow, FCT fibrocartilage tissue, CT cartilaginous tissue, M muscle, G gap, HC hyaline cartilage, FT fibrous connective tissue, Os osteon, CC chondrocyte, OC osteocyte, OB old bone, CB chondroblast, SCR scaffold residue. Stained with H&E

We used 3D printing to fabricate the PLA/PCL/HA scaffold. There are two direct and indirect methods in constructing appropriate macro-and micro-structures. The indirect technique takes a longer time than the direct technique to fabricate the scaffold. It is because the sublimation of the solvent in indirect technique requires freeze-drying. On the other hand, there is a shortcoming in the direct techniques because of restriction of the desired and stability features of the scaffold (Hribar et al. 2014; Do et al. 2015).

The focus of this investigation was to show the effect of BMSCs-seeded onto the PLA/PCL/HA scaffold on bone regeneration. A successful regeneration depended on differentiation of the BMSCs which were seeded onto the PLA/PCL/HA scaffold, into osteocytes, and osteoblasts. Poor cell differentiation, proliferation, and migration and inefficient conversion of these cells to the osteogenic precursor cells result in an incomplete bone healing, delayed union, and malunion or non-union (Harada et al. 2014; Oryan et al. 2017c). HA enhanced bone healing by promoting mesenchymal stem cell

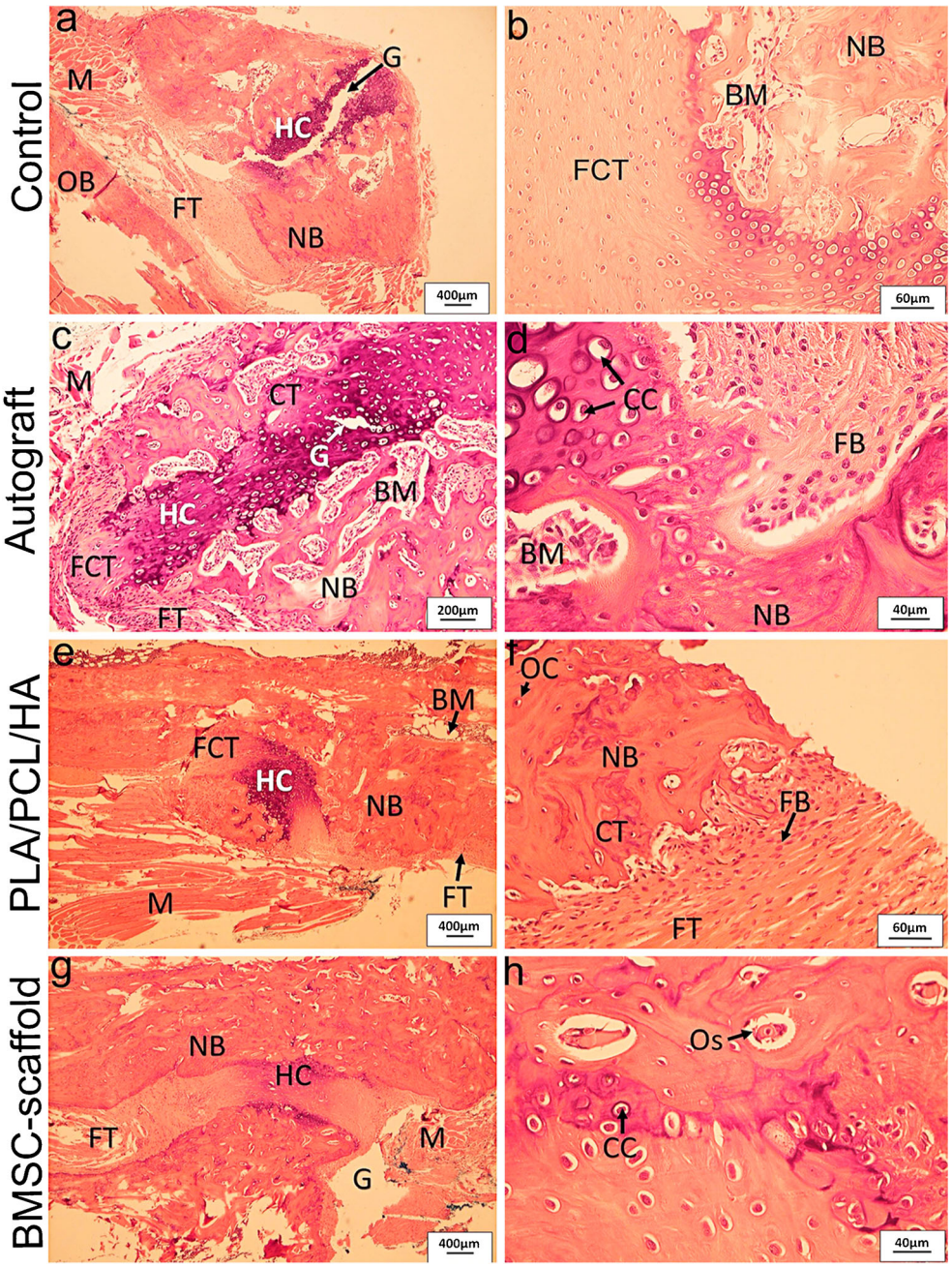

Fig. 6 Histopathological sections of the defects in the radius bone of rats after 80 days post-surgery (a–h). The scaffold implanted in the defect region was degraded and replaced by new fibrous, cartilage, and bone tissue. The highest similarity of the histopathological sections was between the autograft and the BMSCs-seeded PLA/PCL/HA group, and the defects in the animals of these two groups were thoroughly filled with new cartilage and bone tissues. NB new bone, BM bone marrow, FCT fibrocartilage tissue, CT cartilaginous tissue, M muscle, G gap, HC hyaline cartilage, FT fibrous connective tissue, Os osteon, CC chondrocyte, OC osteocyte, OB old bone, CB chondroblast, SCR scaffold residue. Stained with H&E

Table 5 Histomorphometric finding of the defect site after 80 days of surgery. One-way ANOVA followed by Tukey post hoc test ($P < 0.01$ (1 vs. 2, 3, 4), $P < 0.05$ (2 vs. 3))

	Mean ± SD					
Values	FB ± FC	CB ± CC	OB ± OC	Osteoclast	Osteon	Blood vessels
Control (1)	179.12 ± 22.51	8.66 ± 3.49	6.33 ± 0.85	0	0	14.66 ± 4.77
Autograft (2)	7.33 ± 3.31	27.33 ± 3.14	214.59 ± 23.66	3.12 ± 1.10	6 ± 0.84	5 ± 1.68
PLA/PCL/HA (3)	14.34 ± 4.23	21.66 ± 2.99	170.12 ± 4.44	1.22 ± 0.97	4 ± 1.68	7.33 ± 2.11
BMSCs-PLA/PCL/HA (4)	8.45 ± 4.12	25.10 ± 3.43	197 ± 10.68	2.93 ± 0.97	5 ± 1.68	6 ± 1.68

FB, fibroblast; *FC*, fibrocyte; *CB*, chondroblast; *CC*, chondrocyte; *OB*, osteoblast; *OC*, osteocyte

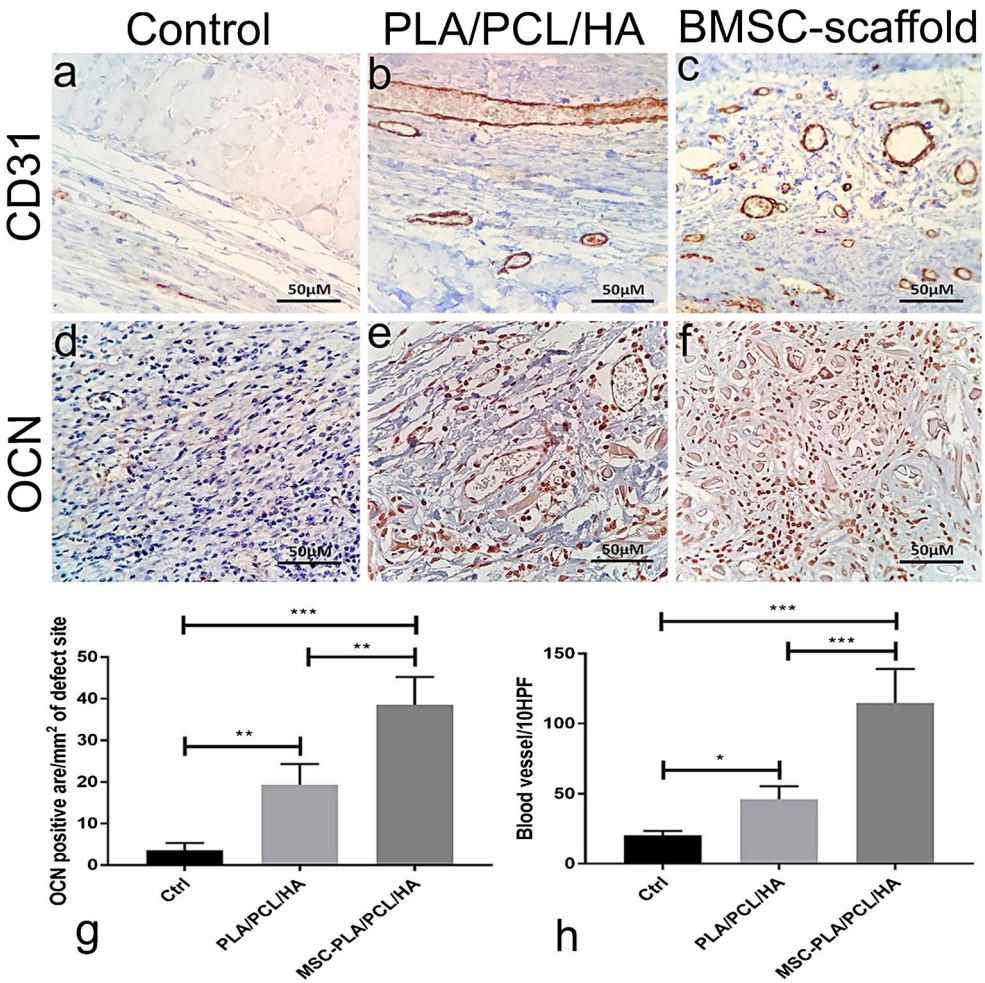

Fig. 7 Immunostaining of the injured area in different experimental groups for bone regeneration and angiogenesis (a–f). Immunohistochemical analysis (g–h) of the OCN and CD31 genes was used to determine the osteogenesis and angiogenesis in samples. The brown color represents positive staining for OCN, and CD31. *, **, ***: values indicate the significant differentiation in comparison to the control group, $*P < 0.05$, $**P < 0.01$, $***P < 0.001$

differentiation to osteoblasts and osteocytes and their migration to enhance collagen synthesis (Chatterjee et al. 2010; Shahsavari-Pour et al. 2018).

In our study, we could demonstrate the angiogenic and osteoinductivity of PLA/PCL/HA scaffold by qRT-PCR by upregulation of the CD31, OPN, and OCN markers. Gene expression of the OCN, a late osteoblastic marker, highlighted the osteogenic superiority in the BMSCs-PLA/PCL/HA group. Sukanya and Mohanan (Sukanya and Mohanan 2018) confirmed cell survival by DNA ladder assay and cell cycle analysis and stated that no apoptosis was seen in the BMSCs of the rat after they were exposed to the degraded PCL products. Besides, the PCL surface was a proper area for cell adherence, and the BMSCs were not destroyed after they differentiated to osteoblasts. The hemocompatibility and non-toxicity of PCL and its degraded products were also confirmed in the same study (Liuac et al. 2013). The BMSCs significantly enhance the degradation rate of the scaffold by secretion of the specific extracellular matrix ingredients (Oryan et al. 2018). It has been shown that richer ECM increases the area of mineralization and ALP activity and gene expression of some osteogenic markers such as Runx-2, Col 1a1, BMP-2, OSX, and b-FGF. Liuac and colleagues revealed that application of the BMSC sheet, in vitro, provided better conditions for bone healing compared with the untreated animals (Chatterjee et al. 2010).

We exhibited the potential of this fabricated scaffold on bone healing by implanting it in a critical-sized defect of the radius in rat. The CT scan images and radiographs revealed that complete union occurred just inside the cell-seeded scaffold and autograft groups after 80 days post-surgery. The cell-free scaffold group demonstrated more superior healing stages than the empty defect. Based on the histopathologic observation, the defect in the control group was not replaced with bone tissue. Endochondral ossification was the characteristic of the BMSCs-seeded, autograft, and cell-free scaffold groups. Finally, the best result in the histopathology interpretation was seen in the autograft and BMSCs-loaded scaffold groups in which the defects were filled with the remodeled compact bone. We demonstrated the scaffolds' biodegradability by a reduction in the size of the scaffold at 40 and 80 days post-operation. The histopathologic study revealed that there was no inflammatory cell infiltration on days 40 and 80 following implantation of the PLA/PCL/HA scaffold. A superior

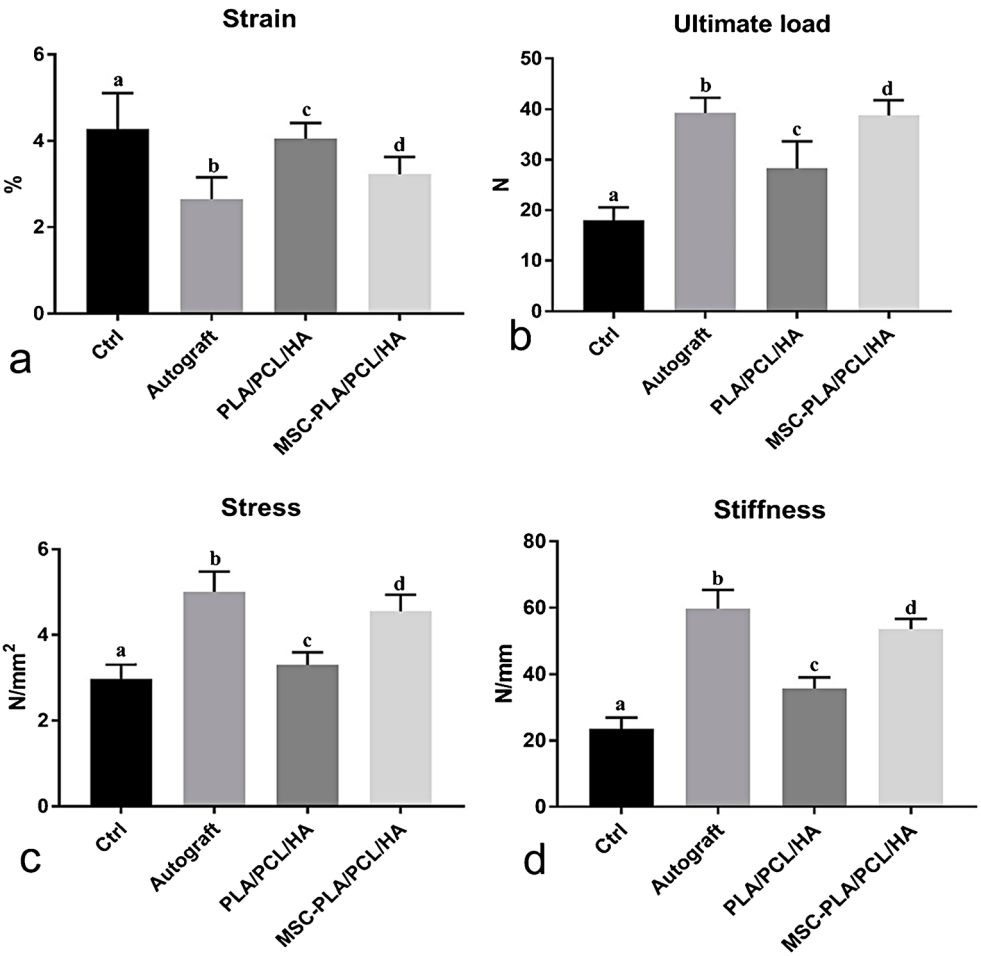

Fig. 8 Biomechanical analysis on the 80th day post-operation (a–d). Ultimate load: $P < 0.01$ (a vs. b and d), $P < 0.05$ (a vs. c), (c vs. b and d). Strain: $P < 0.001$ (a vs. b and d), $P < 0.01$ (a vs. c), (c vs. b and d). Stress: $P < 0.01$ (a vs. b and d), (c vs. b and d). Stiffness: $P < 0.001$ (a vs. b and d), $P < 0.01$ (a vs. c), (c vs. b and d)

newly bone formation was observed in both the autograft and cell-seeded groups by IHC and histomorphometric analysis. The IHC analysis revealed expression of the CD31 marker in the BMSCs-loaded scaffold group and had a significant difference to the cell-free scaffold group ($P < 0.001$) and there was a significant difference in the OC expression between the BMSCs-loaded and cell-free scaffolds ($P < 0.01$). Therefore, based upon radiology, histopathology, and IHC analysis, there were significant differences between the BMSCs-loaded and cell-free scaffold groups, which were defined by the BMSCs-enhanced healing and ability to promote the replacement of empty defects with bone-like tissue.

Implantation of BMSCs on the calcinated cancellous bone resulted in enhanced angiogenesis and improved new bone formation in comparison with healing without using BMSCs (Weiab et al. 2017). BMSCs have a self-renewal capability and differentiate into various cell lineages such as osteoblasts, adipocytes, and chondrocytes (Tsai and Li 2017). Therefore, BMSCs could be used in tissue engineering (cell-based therapy) as a suitable cell source. Zhang et al. revealed that the BMSCs-laden hydrogel established an appropriate micro-environment that resulted in enhanced cell differentiation, attachment, and proliferation in vitro and increased bone healing in vivo (Zhang et al. 2019b).

The load-bearing function would be higher when compact bone and cancellous bone are formed (Henkel et al. 2013). In this experiment, it was showed that the BMSCs-seeded scaffold group had no significant difference with autograft in the maximum load of the injured bone at 80 days post-injury. The fabricated scaffold established a suitable environment via its porosity and materials for cell proliferation and growth. It is necessary to design further studies on the PLA/PCL/HA scaffold with the osteoinductive components to see if they result in significant bone regeneration.

Conclusion

The well-designed PLA/PCL/HA scaffold revealed a reliable therapeutic tool in both in vitro and in vivo conditions according to the characterization of its materials. Also, BMSCs could grow and differentiate to osteogenic precursor cells which could further proliferate, differentiate, and migrate in the scaffold and secrete new bone tissue. Therefore, our results

showed that the bone regenerative capacity of the scaffold was improved when the BMSCs were seeded onto the PLA/PCL/HA scaffold.

Funding This study was supported by the Veterinary School, Shiraz University, Shiraz, Iran. The authors would also like to thank the INSF (grant number 96006039) for its financial support.

Compliance with ethical standards

Conflict of interest The authors declare that they have no conflict of interest.

Animal rights statement This study was approved by the local Ethics Committee of "Regulations in using animals in scientific procedures" in the School of Veterinary Medicine of our University and all rats gained humane care that followed the Guide for Care and Use of Laboratory Animals published by the National Institutes of Health (NIH Publication No. 85-23, revised 1985).

References

Alidadi S, Oryan A, Bigham-Sadegh A, Moshiri A (2017) Comparative study on the healing potential of chitosan, polymethylmethacrylateand demineralized bone matrix in radial bone defects of rat. Carbohydr Polym 166:236–248

Babczyk P, Conzendorf C, Klose J, Schulze M, Harre K, Tobiasch E (2014) Stem cells on biomaterials for synthetic grafts to promote vascular healing. J Clin Med 3:39–87

Bassi A, Gough J, Zakikhani M, Downes S (2011) The chemical and physical properties of poly(ε-caprolactone) scaffolds functionalised with poly(vinyl phosphonic acid-co-acrylic acid). J Tissue Eng 2011:615328

Busilacchi A, Gigante A, Mattioli-Belmonte M, Manzotti S, Muzzarelli RA (2013) Chitosan stabilizes platelet growth factors and modulates stem cell differentiation toward tissue regeneration. Carbohydr Polym 98:665–676

Chatterjee K, Lin-Gibson S, Wallace WE, Parekh SH, Lee YJ, Cicerone MT, Young MF, Simon CG (2010) The effect of 3D hydrogel scaffold modulus on osteoblast differentiation and mineralization revealed by combinatorial screening. Biomaterials 31:5051–5062

Cui Z, Wright LD, Guzzo R, Freeman JW, Drissi DH, Nair LS (2014) Poly(d-lactide)/poly(caprolactone) nanofiber-thermogelling chitosan gel composite scaffolds for osteochondral tissue regeneration in a rat model. J Bioact Compat Polym 28:115–125

Do AV, Khorsand B, Geary SM, Salem AK (2015) 3D printing of scaffolds for tissue regeneration applications. Adv Healthc Mater 4: 1742–1762

Eftekhari H, Jahandideh A, Asghari A, Akbarzadeh A, Hesaraki S (2018) Histopathological evaluation of polycaprolactone nanocomposite compared with tricalcium phosphate in bone healing. J Vet Res 62:385–394

Eshraghi S, Das S (2012) Micromechanical finite element modeling and experimental characterization of the compressive mechanical properties of polycaprolactone: hydroxyapatite composite scaffolds prepared by selective laser sintering for bone tissue engineering. Acta Biomater 8:3138–3143

Fang J, Li P, Lu X, Fang L, Lü X, Ren F (2019) A strong, tough, and osteoconductive hydroxyapatite mineralized polyacrylamide/dextran hydrogel for bone tissue regeneration. Acta Biomater 1(88):503–513

Fu X, Liu G, Halim A, Ju Y, Luo Q, Song G (2019) Mesenchymal stem cell migration and tissue repair. Cells 8:784–800

Götz W, Tobiasch E, Witzleben S, Schulze M (2019) Effects of silicon compounds on biomineralization, osteogenesis, and hard tissue formation. Pharmaceutics 11:117–143

Gregor A, Filová E, Novák M, Kronek J, Chlup H, Buzgo M, Blahnová V, Lukášová V, Bartoš M, Neèas A, Hošek J (2017) Designing of PLA scaffolds for bone tissue replacement fabricated by ordinary commercial 3D printer. J Biol Eng 11:31–51

Guntillake PA, Adhikari R (2003) Biodegradable synthetic polymers for tissue engineering. Eur Cell Mater 5:1–16

Harada N, Watanabe Y, Sato K, Abe S, Yamanaka K, Sakai Y, Kaneko T, Matsushita T (2014) Bone regeneration in a massive rat femur defect through endochondral ossification achieved with chondrogenically differentiated MSCs in a degradable scaffold. Biomaterials 35(27): 7800–7810

Hashimoto Y, Nishida Y, Takahashi S, Nakamura H, Mera H, Kashiwa K, Yoshiya S, Inagaki Y, Uematsu K, Tanaka Y, Asada S, Akagi M, Fukuda K, Hosokawa Y, Myoui A, Kamei N, Ishikawa M, Adachi N, Ochi M, Wakitani S (2019) Transplantation of autologous bone marrow-derived mesenchymal stem cells under arthroscopic surgery with microfracture versus microfracture alone for articular cartilage lesions in the knee: a multicenter prospective randomized control clinical trial. Regen Ther 11:106–113

Hassanajili S, Karami-Pour A, Oryan A, Talaei-Khozani T (2019) Preparation and characterization of PLA/PCL/HA composite scaffolds using indirect 3D printing for bone tissue engineering. Mater Sci Eng C 104:1099960

Henkel J, Woodruff MA, Epari DR, Steck R, Glatt V, Dickinson IC, Choong PFM, Schuetz MA, Hutmacher DW (2013) Bone regeneration based on tissue engineering conceptions-a 21st century perspective. Bone Res 1(3):216–248

Hou W, Ye C, Chen M, Li W, Gao X, He R, Zheng Q, Zhang W (2019) Bergenin activates SIRT1 as a novel therapeutic agent for osteogenesis of bone mesenchymal stem cells. Front Pharmacol 10:618–629

Hribar KC, Soman P, Warner J, Chung P, Chen S (2014) Light-assisted direct-write of 3D functional biomaterials. Lab Chip 14:268–275

Inzana JA, Olvera D, Fuller SM, Kelly JP, Graeve OA, Schwarz EM, Kates SL, Awad HA (2014) 3D printing of composite calcium phosphate and collagen scaffolds for bone regeneration. Biomaterials 35: 4026–4034

Jensen A, Reolfing HD, Le DQS, Kristiansen AA, Nygaard JV, Hokland LB (2013) Surface-modified functionalized polycaprolactone scaffolds for bone repair: in vitro and in vivo experiments. J Biomed Mater Res 102:2993–3003

Kamath MS, Ahmed SSJ, Dhanasekaran M, Santosh S (2014) Polycaprolactone scaffold engineered for sustained release of resveratrol: therapeutic enhancement in bone tissue engineering. Int J Nanomedicine 9:183–195

Kumar P, Dehiya BS, Sindhu A (2018) Bioceramics for hard tissue engineering applications: a review. Int J Appl Eng Res 13(5):2744–2752

Leonga KF, Chuaa CK, Sudarmadjia N, Yeonga WY (2008) Engineering functionally graded tissue engineering scaffolds. J Mech Behav Biomed Mater 1:140–152

Lima Cavalcanti JH, Matos PC, Depes de Gouvea CV, Carvalho W, Calvo-Guirado JL, Aragoneses JM, Perez-Diaz L, Gehrke SA (2019) In vitro assessment of the functional dynamics of titanium with surface coating of hydroxyapatite nanoparticles. Materials 12(5):840–853

Liuac Y, Ming L, Luo H, Liu W, Zhang Y, Liu H, Jin Y (2013) Integration of a calcined bovine bone and BMSC-sheet 3D scaffold and the promotion of bone regeneration in large defects. Biomaterials 34(38):9998–10006

Lopes MS, Jardini AL, Maciel R (2012) Poly(lactic acid) production for tissue engineering applications. Proc Eng 42:1402–1413

Luo CH, Fang H, Zhou M, Li J, Zhang X, Liu SH, Zhou CH, Hou J, He H, Sun J, Wang ZH (2019) Biomimetic open porous structured core-shell microtissue with enhanced mechanical properties for bottom-up bone tissue engineering. Theranostics 9:4663–4677

Marins NH, Lee BEJ, Silva RM, Raghavan A, Villarreal-Carre NL, Grandfield K (2019) Niobium pentoxide and hydroxyapatite particle loaded electrospun polycaprolactone/gelatin membranes for bone tissue engineering. Colloids Surf B: Biointerfaces 182:110386

Misra SK, Ansari T, Mohn D, Valappil SP, Brunner TJ, Stark WJ, Roy I, Knowles JC, Sibbons PD, Jones EV, Boccaccini AR, Salih V (2009) Effect of nanoparticulate bioactive glass particles on bioactivity and cytocompatibility of poly(3-hydroxybutyrate) composites. J R Soc Interface 7:453–465

Mitsak AG, Kemppainen JM, Harris MT, Hollister ST (2011) Effect of polycaprolactone scaffold permeability on bone regeneration in vivo. Tissue Eng Part A 17:1831–1839

Moghadam MZ, Hassanajili S, Esmaeilzadeh F, Ayatollahi M, Ahmadi M (2017) Formation of porous HPCL/LPCL/HA scaffolds with supercritical CO_2 gas foaming method. J Mech Behav Biomed Mater 69:115–127

Mondal D, Griffith M, Venkatraman SS (2016) Polycaprolactone-based biomaterials for tissue engineering and drug delivery: current scenario and challenges. Int J Polym Mater Polym Biomater 65:255–265

Moshiri A, Oryan A, Meimandi-Parizi A (2013) Role of tissue-engineered artificial tendon in healing of a large achilles tendon defect model in rabbits. Coll Surg 217:421–441

Mou ZL, Zhao LJ, Zhang QA, Zhang J, Zhang ZQ (2011) Preparation of porous PLGA/HA/collagen scaffolds with supercritical CO2 and application in osteoblast cell culture. J Supercrit Fluids 58(3):398–406

Oryan A, Alidadi S (2018) Reconstruction of radial bone defect in rat by calcium silicate biomaterials. Life Sci 201:45–53

Oryan A, Meimandi-Parizi A, Shafiei-Sarvestani Z, Bigham AS (2012) Effects of combined hydroxyapatite and human platelet rich plasma on bone healing in rabbit model: radiological, macroscopical, hidtopathological and biomechanical evaluation. Cell Tissue Bank 13:639–651

Oryan A, Alidadi S, Moshiri A, Maffulli N (2014) Bone regenerative medicine:classic options, novel strategies, and future directions. J Orthop Surg Res 9:18

Oryan A, Alidadi S, Bigham-Sadegh A, Meimandi-Parizi A (2017a) Chitosan/gelatin/platelet gel enriched by a combination ofhydroxyapatite and beta-tricalcium phosphate in healing of a radialbone defect model in rat. Int J Biol Macromol 101:630–637

Oryan A, Kamali A, Moshiri A, Baghaban-Eslaminejad M (2017b) Role of mesenchymal stem cells in bone regenerative medicine: what is the evidence? Cells Tissues Organs 204(2):59–83

Oryan A, Alidadi S, Bigham-Sadegh A, Moshiri A, Kamali A (2017c) Effectiveness of tissue engineered chitosan-gelatin composite scaffold loaded with human platelet gel in regeneration of critical sized radial bone defect in rat. Corel 254:65–77

Oryan A, Baghaban-Eslaminejad M, Kamali A, Hosseini S, Sayahpour FA, Baharvand H (2018) Synergistic effect of strontium, bioactive glass and nano-hydroxyapatite promotes bone regeneration of critical-sized radial bone defects. J Biomed Mater Res Part B 107(1):50–64

Ostafinska A, Fortelny I, Nevoralova M, Hodan J, Kredatusova J, Slouf M (2015) Synergistic effects in mechanical properties of PLA/PCL blends with optimized composition, processing, and morphology. RSC Adv 5:98971–98982

Ottensmeyer P, Witzler M, Schulze M, Tobiasch E (2018) Small molecules enhance scaffold-based bone grafts via purinergic receptor signaling in stem cells. Int J Mol 19:3601–3630

Papadimitropoulos A, Riboldi SA, Tonnarelli B, Piccinini E, Woodruff MA, Hutmacher DW, Martin I (2013) A collagen network phase improves cell seeding of open pore structure scaffolds under perfusion. J Tissue Eng Regen Med 7:183–191

Peter M, Binulal N, Nair S, Selvamurugan N, Tamura H, Jayakumar R (2010) Protein growth factors loaded highly porous chitosan scaffold: a comparisonof bone healing properties. Chem Eng J 158:353–361

Pilia M, Guda T, Appleford M (2013) Development of composite scaffolds for load-bearing segmental bone defects. Biomed Res Int 2013:458253

Pizzicannella J, Diomede F, Gugliandolo A, Chiricosta L, Bramanti P, Merciaro I, Orsini T, Mazzon E, Trubiani O (2019) 3D printing PLA/gingival stem cells/EVs upregulate miR-2861 and -210 during osteoangiogenesis commitment. Int J Mol Sci 20:3256–3274

Ramtani S (2004) Mechanical modeling of cell/ECM and cell/cell interactions during the contraction of a fibroblast-populated collagen microsphere: theory and model simulation. J Biomech 37(11):1709–1718

Raucci MG, Guarino V, Ambrosio L (2010) Effect of calcium precursors and pH on the precipitation of carbonated hydroxyapatite. Compos Sci Technol 70:1861–1868

Roohani-Esfahani S, Nouri-Khorasani S, Lu Z, Appleyard R, Zreiqat H (2011) Effects of bioactive glass nanoparticles on the mechanical and biological behavior of composite coated scaffolds. Acta Biomater 7(3):1307–1318

Schumacher M, Uhl F, Detsch R, Deisinger U, Ziegler G (2010) Static and dynamic cultivation of bone marrow stromal cells on biphasic calcium phosphate scaffolds derived from an indirect rapid prototyping technique. J Mater Sci Mater Med 21:3039–3048

Shahrezaee M, Raz M, Shishehbor S, Moztarzadeh F, Baghbani F, Sadeghi A, Bajelani K, Tondnevis F (2018a) Synthesis of magnesium doped amorphous calciumphosphate as a bioceramic for biomedical application: invitro study. Silicon 10:1171–1179

Shahrezaee M, Salehi M, Keshtkari S, Oryan A, Kamali A, Shekarchi B (2018b) In vitro and in vivo investigation of PLA/PCL scaffold coated with metformin-loaded gelatin nanocarriers in regeneration of criticalsized bone defects. Nanomed Nanotechnol Biol Med 14:2061–2073

Shahrezaie M, Moshiri A, Shekarchi B, Oryan A, Maffulli N, Parvizi J (2017) Effectiveness of tissue engineered three dimensional bioactive graft on bone healing and regeneration: an in vivo study with significant clinical value. J Tissue Eng Regen Med 12(4):936–960

Shahsavari-Pour S, Aliabadi E, Latifi M, Zareifard N, Namavar MR, Talaei-Khozani T (2018) Evaluation of the possible synergic regenerative effects of platelet-rich plasma and hydroxyapatite/zirconia in the rabbit mandible defect model. Iran J Med Sci 43:633–644

Shimojo AAM, Perez AGM, Galdames SEM, Brissac ICDS, Santana MHA (2015) Performance of PRP associated with porous chitosan as acomposite scaffold for regenerative medicine. Sci World J 2015:396131

Siddiqui N, Asawa S, Birru B, Baadhe R, Rao S (2018) PCL based composite scaffold matrices for tissue engineering applications. Mol Biotechnol 60(7):506–532

Sivashankari P, Prabaharan M (2016) Prospects of chitosan-based scaffolds forgrowth factor release in tissue engineering. Int J Biol Macromol 93:1382–1389

Solgi S, Shahrezaee M, Zamanian A, Jafarzadeh kasha TS, Raz M, Khoshroo K, Tahriri M (2015) Sol-gel synthesis and characterization of SiO_2-Cao-P_2O_5-SrO bioactive glass: in vitro study. Key Eng Mater 631:30–35

Sukanya VS, Mohanan PV (2018) Degradation of poly(ε-caprolactone) and bio-interactions with mouse bone marrow mesenchymal stem cells. Colloids Surf B: Biointerfaces 163:107–118

Torres AL, Gaspar VM, Serra IR, Diogo GS, Fradique R, Silva AP, Correia IJ (2013) Bioactive polymeric-ceramic hybrid 3D scaffold for application in bone tissue regeneration. Mat Sci Eng C Mater 33(7):4460–4469

Tsai TL, Li WJ (2017) Identification of bone marrow-derived soluble factors regulating human mesenchymal stem cells for bone regeneration. Stem Cell Rep J 8:387–400

Vergroesen PPA, Kroeze RJ, Helder MN, Smit TH (2011) The use of poly(L-lactide-co-caprolactone) as a scaffold for adipose stem cells in bone tissue engineering: application in a spinal fusion model. Macromol Biosci 11:722–730

Wang J, Wu D, Zhang Z, Li J, Shen Y, Wang Z, Li Y, Zhang ZY, Sun J (2015) Biomimetically ornamented rapid prototyping fabrication of an apatite-collagen-polycaprolactone composite construct with nano-micro-macro hierarchical structure for large bone defect treatment. ACS Appl Mater Interfaces 7:26244–26256

Weiab J-Q, Xue-Hui Y, Wei-Wei Z, Tuan-Feng L, Hua Z, Deng ZXL (2017) Enhanced critical-sized bone defect repair efficiency by combining deproteinized antler cancellous bone and autologous BMSCs. Chin Chem Lett 28(4):845–850

Witzler M, Ottensmeyer P, Gericke M, Heinz T, Tobiasch E, Schulze M (2019) Non-cytotoxic agarose/hydroxyapatite composite scaffolds for drug release. Int J Mol Sci 20:3565–3583

Woodruff MA, Hutmacher DW (2010) The return of a forgotten polymer-polycaprolactone in the 21st century. Prog Polym Sci 35:1217–1256

Yu W, Li R, Long J, Chen P, Hou A, Li L, Sun X, Zheng G, Meng H, Wang Y, Wang A, Sui X, Guo Q, Tao S, Peng J, Qin L, Lu S, Lai Y (2019) Use of a three-dimensional printed polylactide-coglycolide/tricalcium phosphate composite scaffold incorporating magnesium powder to enhance bone defect repair in rabbits. J Orthop Translat 16:62–70

Yun HS, Park JW, Kim SH, Kim YJ, Jang JH (2010) Effect of the pore structure of bioactive glass balls on biocompatibility in vitro and in vivo. Acta Biomater 7:2651–2660

Zhang ZZ, Zhang HZ, Zhang ZY (2019a) 3D printed poly(ε-caprolactone) scaffolds function with simvastatin loaded poly(lactic.Co.glycolic acid) microspheres to repair load bearing segmental bone defects. Exp Ther Med 17:79–90

Zhang Y, Chen H, Zhang T, Zan Y, Ni T, Cao Y, Wang J, Liu M, Pei R (2019b) Injectable hydrogels from enzyme-catalyzed crosslinking as BMSCs-laden scaffold for bone repair and regeneration. Mater Sci Eng C 96:841–849